Modeling the optical properties of mineral particles suspended in seawater and their influence on ocean reflectance and chlorophyll estimation from remote sensing algorithms

Sławomir B. Woźniak and Dariusz Stramski

The optical properties of mineral particles suspended in seawater were calculated from the Mie scattering theory for different size distributions and complex refractive indices of the particles. The ratio of the spectral backscattering coefficient to the sum of the spectral absorption and backscattering coefficients of seawater, $b_b(\lambda)/[a(\lambda) + b_b(\lambda)]$, was analyzed as a proxy for ocean reflectance for varying properties and concentrations of mineral particles. Given the plausible range of variability in the particle size distribution and the refractive index, the general parameterizations of the absorption and scattering properties of mineral particles and their effects on ocean reflectance in terms of particle mass concentration alone are inadequate. The variations in the particle size distribution and the refractive index must be taken into account. The errors in chlorophyll estimation obtained from the remote sensing algorithms that are due to the presence of mineral particles can be very large. For example, when the mineral concentration is 1 g m^{-3} and the chlorophyll a concentration is low (0.05 mg m^{-3}), current global algorithms based on a blue-to-green reflectance ratio can produce a chlorophyll overestimation ranging from ~50% to as much as 20-fold.

OCIS codes: 010.4450, 300.1030, 290.1350, 350.4990, 010.0010.

1. Introduction

Suspended mineral particles can play an important role in ocean optical properties, including the spectral reflectance (ocean color), because such particles can be abundant in seawater, they scatter light efficiently owing to their high refractive index relative to that of water, and their absorption of light is generally not negligible.[1,2] Significant concentrations of minerals are common in coastal waters where large amounts of suspended particles are discharged from rivers or other sources, such as bottom resuspension and shore erosion by wave action.[3,4] In such waters mineral particles can dominate the optical properties. Mineral concentrations in water typically decrease with distance from land. However, even the open-ocean waters far beyond the continental shelves can receive a significant input of mineral particles owing to long-range atmospheric transport and subsequent deposition of aeolian dust that originates from distant desert and semiarid regions on Earth.[5] An adequate knowledge of mineral particle properties and concentrations is necessary for an understanding of ocean optical properties and for various oceanographic applications of optical measurements, including remote sensing. This knowledge is important not only for optically complex coastal waters but also for ocean waters whose optical properties have been traditionally assumed to be dominated by phytoplankton and covarying materials.[6,7]

The inherent optical properties (IOPs) of mineral suspensions have been little investigated, and the variability in these properties is still poorly quantified. Only recently were comprehensive experiments initiated to measure the spectral absorption and scattering properties of different assemblages of mineral particles suspended in water.[1,2] These studies demonstrated that the mass-specific absorp-

When this research was performed, S. B. Woźniak (woznjr@iopan.gda.pl) was with the Marine Physical Laboratory, Scripps Institution of Oceanography, University of California at San Diego, La Jolla, California 92093-0238. He is now with the Institute of Oceanology, Polish Academy of Sciences, Powstańców Warszawy 55, 81-712 Sopot, Poland. D. Stramski is with the Marine Physical Laboratory, Scripps Institution of Oceanography, University of California at San Diego, La Jolla, California 92093-0238.

Received 18 September 2003; revised manuscript received 17 March 2004; accepted 24 March 2004.

0003-6935/04/173489-15$15.00/0

tion and scattering coefficients of mineral suspensions can vary significantly (severalfold) owing to variations in the chemical and mineralogical composition as well as in the size distribution of particulate assemblages. With regard to the influences of minerals on apparent optical properties (AOPs) such as reflectance, several studies reported reflectance measurements for different assemblages of suspended minerals contained in the tank.[8–12] Although the AOP measurements in the tank have a limited value for representing natural water bodies, these experiments showed that reflectance variability can be associated not only with variations in the mineral mass concentration but also with changes in the type and size of mineral particles.

Satellite remote sensing of ocean reflectance is a unique tool for studying environmental processes in the upper ocean over extended spatial and temporal scales that is unmatched by traditional oceanographic techniques for data collection. In the past years these applications have been focused on the estimation of chlorophyll *a* concentration (*Chl*). Nevertheless, there has also been a significant effort to develop algorithms for retrieving the concentration of suspended particulate matter (SPM), especially in coastal waters. In principle, SPM includes both the minerogenic and organic particles but, in coastal and inland aquatic environments, SPM can often be dominated by inorganic particles. The ocean color algorithms for estimating SPM[11,13–16] or both SPM and *Chl* (and possibly other data products such as optical properties of water)[17–21] have been proposed for various coastal environments. The performance of the algorithms is often considerably degraded owing to the optical complexity of coastal waters. The reasons for the difficulties include failure of the traditional oversimplified representation of water composition in terms of only a few broadly defined constituents [typically phytoplankton, suspended sediments, and colored dissolved organic matter (CDOM)], inadequate *a priori* knowledge of or set of assumptions about the mass-specific optical coefficients for water constituents, and lack of (or weak) correlation between the concentration of chlorophyll and nonchlorophyllous water constituents. In reality, each of the broadly defined water constituents may exhibit significant optical variability due to variations in species composition, particle size, shape, and refractive index.

Theoretical analyses have been used to advance an understanding of the variations in reflectance that are caused by the presence of mineral particles.[22,23] These models considered a restricted range of variability in mineral properties, assuming no absorption by particles and single Junge-type particle size distribution with a slope of -4. Other studies suggested that reflectance in turbid waters can be assumed as being independent of particle size distribution.[24,25] In reality, however, various coastal environments are likely to exhibit significant variations in the composition of mineral species (and hence the real and imaginary parts of the refractive index) as well as in the particle size distribution. Therefore a systematic study of the variations in the IOPs of mineral assemblages and in the spectral reflectance, which are produced by a wide range of mineral particle properties at varying particle concentrations, is required. In addition, there is a need to examine how the variations in mineral properties and concentrations affect the estimation of chlorophyll concentration from reflectance. The limited amount of quantitative results suggests that the mineral-induced errors in the *Chl* estimation can be of the order of tens of percent or more.[15] The problem may be especially important in clear waters with low *Chl* and with significant input of mineral dust originating, for example, from atmospheric deposition.[26]

In this study we use a simplified model that combines Mie scattering calculations of the optical properties of hypothetical assemblages of mineral particles suspended in water and the analysis of the ratio of the backscattering coefficient to the sum of absorption and backscattering coefficients of seawater as a proxy for ocean reflectance. Our objectives are to show how variations in the size distribution and complex refractive index of mineral particles affect the mass-specific optical coefficients of these particles and how these properties of mineral particles affect the spectral reflectance at varying particle concentrations. We also examine the sensitivity of NASA's standard chlorophyll algorithms that are used in conjunction with satellite missions involving SeaWiFS (Sea-viewing Wide Field-of-view Sensor) and MODIS (Moderate-resolution Imaging Spectroradiometer) sensors to the concentration and properties of mineral assemblages.

2. Description of the Model

A. Approach

Our modeling approach is presented in Fig. 1. First, to calculate the optical properties of mineral particles suspended in water, we made several assumptions about the nature of the particles. We assumed that the assemblages of mineral particles consist of homogeneous spheres with a specified size distribution, $N(D)$, between the minimum and the maximum particle diameters, $D_{\min}$ and $D_{\max}$, respectively. $N(D)\mathrm{d}D$ is the number of particles per unit volume of water in the size range from D to $D + \mathrm{d}D$. For each modeled particulate assemblage, we also made an assumption about the spectral behavior of the real and imaginary parts of the refractive index of the particles relative to water, $n(\lambda)$ and $n'(\lambda)$, respectively, where λ is the light wavelength in vacuum. These assumptions allowed us to use the Mie scattering theory adopted to polydisperse assemblages of particles.[27,28] We calculated the spectral efficiency factors for absorption, $\bar{Q}_a(\lambda)$, and backscattering, $\bar{Q}_{bb}(\lambda)$, which essentially represent an average particle derived from the modeled polydisperse particulate assemblage.[29] Then, by combining the calculated efficiency factors and the assumed density of mineral particles, ρ, we obtained the spectral mass-specific

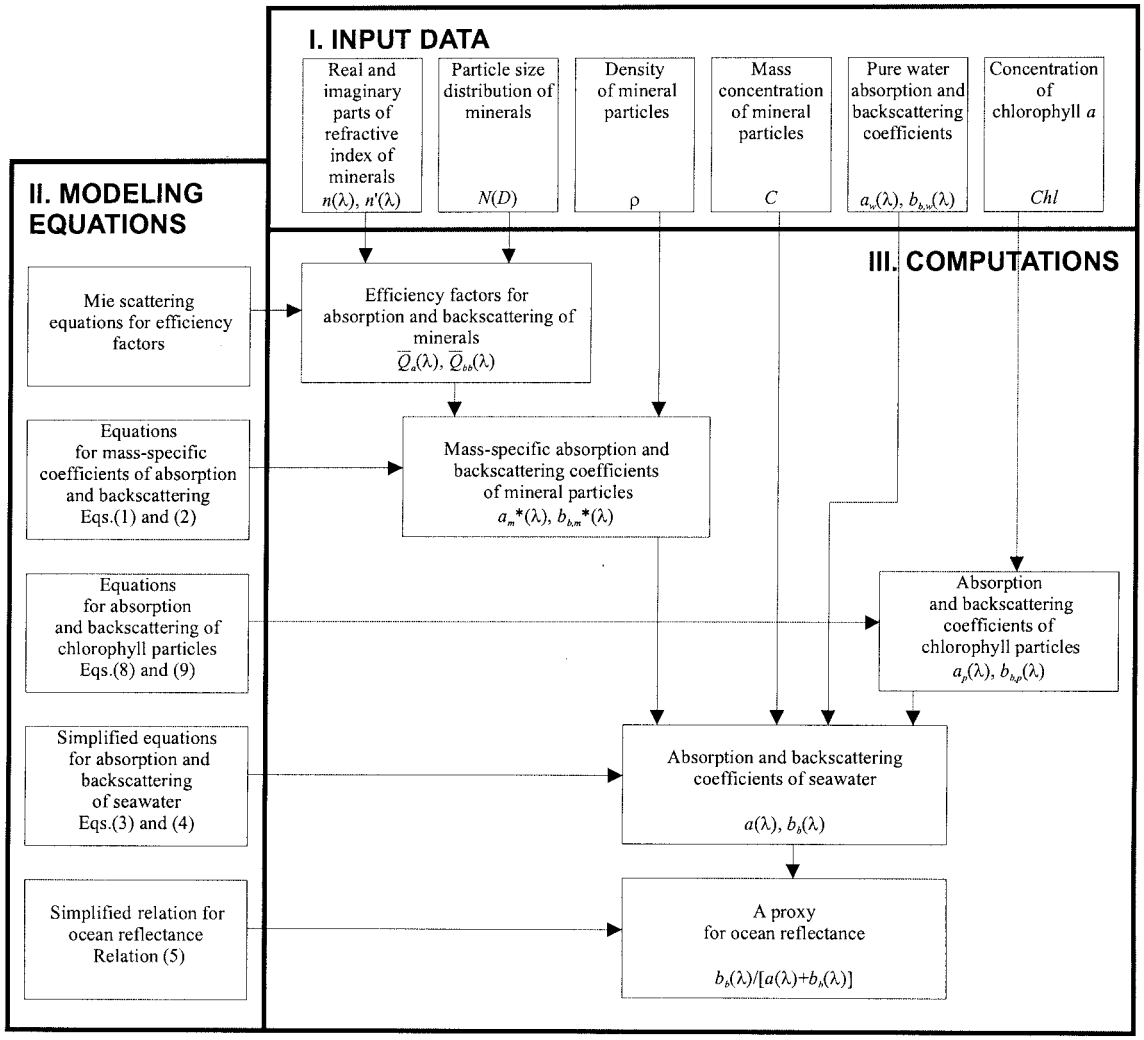

Fig. 1. Block diagram of the model.

coefficients for absorption, $a_m^*(\lambda)$, and backscattering, $b_{b,m}^*(\lambda)$, of mineral assemblages:

$$a_m^*(\lambda) = \frac{3\bar{Q}_a(\lambda)}{2\rho} \frac{\int_{D_{\min}}^{D_{\max}} N(D) D^2 \mathrm{d}D}{\int_{D_{\min}}^{D_{\max}} N(D) D^3 \mathrm{d}D}, \quad (1)$$

$$b_{b,m}^*(\lambda) = \frac{3\bar{Q}_{bb}(\lambda)}{2\rho} \frac{\int_{D_{\min}}^{D_{\max}} N(D) D^2 \mathrm{d}D}{\int_{D_{\min}}^{D_{\max}} N(D) D^3 \mathrm{d}D}. \quad (2)$$

These mass-specific coefficients are defined as the absorption or backscattering coefficients per unit mass concentration of mineral particles. The units of $a_m^*(\lambda)$ and $b_{b,m}^*(\lambda)$ are $\mathrm{m}^2\ \mathrm{g}^{-1}$. Although our analysis is focused on $a_m^*(\lambda)$ and $b_{b,m}^*(\lambda)$, we also obtained results for the mass-specific scattering coefficient $b_m^*(\lambda)$. These results are only briefly reported here because a comprehensive discussion of $b_m^*(\lambda)$ was presented elsewhere.[30]

To study the sensitivity of ocean reflectance to different properties and concentrations of minerals, we applied a simplified model of the IOPs of seawater. We assumed that the absorption and scattering of light is caused by only two or three water components: water itself, suspended mineral particles, and chlorophyll particles that include phytoplankton and other organic particles (both living and nonliving) covarying with chlorophyll concentration. Under this assumption, the total absorption coefficient of seawater, $a(\lambda)$, is the sum of the absorption of pure seawater, $a_w(\lambda)$, the absorption of mineral particles, $a_m(\lambda)$, and the absorption of chlorophyll particles, $a_p(\lambda)$:

$$a(\lambda) = a_w(\lambda) + a_m^*(\lambda) C + a_p(\lambda), \quad (3)$$

where C is the mass concentration of minerals in water (units for C are $\mathrm{g\ m}^{-3}$) and $a_m(\lambda) = a_m^*(\lambda)\, C$.

Similarly, the total backscattering coefficient of seawater, $b_b(\lambda)$, is

$$b_b(\lambda) = b_{b,w}(\lambda) + b_{b,m}^*(\lambda)C + b_{b,p}(\lambda), \qquad (4)$$

where $b_{b,w}(\lambda)$ is the backscattering of pure seawater, $b_{b,p}(\lambda)$ is the backscattering of chlorophyll particles, and $b_{b,m}(\lambda) = b_{b,m}^*(\lambda)\,C$ is the backscattering of mineral particles. The first part of our analysis of reflectance (see Subsection 3.B) is focused just on the effects of mineral particles. Thus, in this analysis, we assume that the optical coefficients in Eqs. (3) and (4) are produced only by the water itself and the mineral particles. The second part of the analysis is focused on the effects of minerals on the chlorophyll estimation from the reflectance under the assumption that the optical coefficients are produced by all three components. In these simplified IOP models we do not account for other optically significant constituents of water such as CDOM and bubbles. This simplification is advantageous because our analysis is not intended as a predictive model or simulation of any natural water body but as a simple research tool for examining the optical effects associated with variations in the properties and concentrations only of mineral particles.

With regard to modeling of ocean reflectance, we assumed that the spectral remote-sensing reflectance just above the sea surface, $R_{rs}(\lambda)$, varies as the ratio of the backscattering coefficient to the sum of the absorption and backscattering coefficients:[31]

$$R_{rs}(\lambda) \propto \frac{b_{b,w}(\lambda) + b_{b,p}(\lambda) + b_{b,m}^*(\lambda)C}{a_w(\lambda) + a_p(\lambda) + a_m^*(\lambda)C + b_{b,w}(\lambda) + b_{b,p}(\lambda) + b_{b,m}^*(\lambda)C}. \qquad (5)$$

The coefficient of the proportionality in this relation (not shown here) may vary to some extent, depending on the illumination conditions (Sun position and sky and sea-surface conditions), the IOPs of water, and the wavelength of light. However, the wavelength dependence is generally weak, so this coefficient can be approximated by a constant value that is independent of λ.[32,33] Therefore we can analyze the spectral values of $b_b/(a + b_b)$ as a proxy for the spectral reflectance. Our interest is in the spectral region from 350 to 750 nm, and all the calculations for the mineral particles were made in this region with a 1-nm interval. The calculations involving the chlorophyll particles were made in the spectral region from 400 to 700 nm with a 1-nm interval.

B. Input Data for the Model

Table 1 shows the mean values of the real part of the refractive index, n, and the density, ρ, for various mineral species taken from the literature.[34,35] As an input to the Mie calculations, we used the three values of n (relative to water): 1.15, 1.18, and 1.22, which represent a range for many common mineral species. We assumed that n is independent of light wavelength. Because the values of n for some common mineral species are lower than 1.15, we made additional Mie calculations with $n = 1.12$ to test the sensitivity of mass-specific optical coefficients to smaller n. To assume the density of minerals for each refractive index, we established the dependence between n and ρ. Based on data for 29 mineral species covering the density range from 2.04×10^6 to 5.09×10^6 g m^{-3}, a general tendency of increasing ρ with n is observed [Figs. 2(a) and 2(b)], which is described by the following linear regression:

$$n = 0.1475 \times 10^{-6}\rho + 0.7717, \qquad (6)$$

with the squared correlation coefficient r^2 of 0.77. From this relation we found that $\rho = 2.57 \times 10^6$ g m^{-3} for $n = 1.15$, $\rho = 2.77 \times 10^6$ g m^{-3} for $n = 1.18$, and $\rho = 3.04 \times 10^6$ g m^{-3} for $n = 1.22$.

Next we selected the spectral values for the imaginary part of the refractive index, $n'(\lambda)$, relative to water. There exists only a limited and uncertain data set for the imaginary index in the visible spectral range for mineral particles.[36] We have chosen to use two different spectra of $n'(\lambda)$: one is referred to as the low-n' (low-absorption) case and the other is the high-n' (high-absorption) case [Fig. 2(c)]. The low-n' case is based on determinations for marine detrital particles.[37] Those determinations established an exponential function $n'(\lambda) = 0.010658 \exp(-0.007186\ \lambda)$. The values of our low-$n'$ spectrum are 25% lower than those predicted by the exponential function (we note that there is a typographical error in the equation for n' on p. 2935 in Ref. 37 and that all calculations for detritus and minerals in Ref. 37 were made with a factor of 0.007954 rather than 0.010658 in the exponential function). The high-n' case is based on data for Saharan dust presented in Patterson *et al.*[38] Specifically, we assumed the n' values that are 25% lower than those derived from the data of Patterson *et al.* (note that the original data in Patterson *et al.* are reported for particles suspended in air). The data of Patterson *et al.* appear to significantly overestimate n' in the red and near-infrared spectral regions, as suggested by recent measurements of very small or undetectable absorption of aqueous suspensions of Saharan dust in these spectral regions.[1] It is thus likely that their data at shorter wavelengths may also be overestimated to some degree; hence we have tentatively taken the values that are 25% lower. We expect that $n'(\lambda)$ for many natural assemblages of mineral particles suspended in water may be between the assumed low- and high-n' cases.

The final input needed to perform the Mie scattering calculations for mineral particles is the size dis-

Table 1. Real Part of the Refractive Index n (Relative to Water) for Various Types of Mineral Particles and the Corresponding Values of the Average Particle Density ρ[a]

Mineral	n	ρ ($\times 10^6$ g m^{-3})
Opal	1.067	2.10
Fluorite	1.070	3.18
Montmorillonite	1.124	2.04
Orthoclase	1.136	2.56
Gypsum	1.137	2.32
Microcline	1.137	2.56
Albite	1.145	2.69
Quartz	1.148	2.63
Oligoclase	1.151	2.69
Halite	1.152	2.16
Kaolinite	1.167	2.60
Gibbsite	1.170	2.40
Illite	1.171	2.85
Talc	1.171	2.82
Calcite	1.173	2.71
Anhydrite	1.184	2.96
Muscovite	1.185	2.85
Dolomite	1.198	2.94
Magnesite	1.206	3.00
Prochlorite (Ripidolite)	1.215	2.80
Aragonite	1.218	2.93
Apatite	1.226	3.15
Hornblende	1.235	3.20
Augite	1.277	3.40
Siderite	1.294	3.96
Corundum	1.308	4.05
Zircon	1.450	4.65
Limonite	1.530	3.80
Chromite	1.578	5.09

[a]The refractive-index values are given according to Kerr.[34] For anisotropic minerals (most of the data in the table), the presented values of n are averages of two or three indices of uniaxial and biaxial minerals, respectively. The density values are given according to Berry and Mason.[35]

tribution of the particles. We assumed the following Junge-type (power-law) differential size distribution:[39]

$$N(D) = KD^j. \tag{7}$$

Because only the shape of the size distribution is important to our Mie calculations, an arbitrary value for the coefficient K can be chosen [$K = 10^4$ in Fig. 2(d)]. The slope j for marine particles in the size range from ~1 μm to several tens of micrometers often assumes the values close to −4. We chose $j = -4$ to represent our base model. We also considered the size distribution with a steeper slope, $j = -4.8$, and the size distribution with a relatively gentle slope, $j = -3.2$ [Fig. 2(d)]. We assumed that the minimum particle diameter, $D_{\min}$, is 0.05 μm and that the maximum diameter, $D_{\max}$, is 500 μm. This generally provides a good approximation of the optically significant size range of the marine particles.[40] However, we made additional Mie calculations with $D_{\max} = 50$ μm and $D_{\max} = 10$ μm to examine the sensitivity of the mass-specific optical coefficients to $D_{\max}$. The consideration of smaller values of $D_{\max}$ is important because the relatively large and heavy mineral particles can efficiently be removed by sinking from the water column. The size distributions of mineral particles with a 5-order-of-magnitude decrease in particle concentration between 1 and 10 μm can easily be produced in laboratory sedimentation experiments.[2]

To calculate $a(\lambda)$ and $b_b(\lambda)$ from Eqs. (3) and (4), we used the literature values for the absorption coefficient of pure seawater, $a_w(\lambda)$,[41,42] and the backscattering coefficient of pure seawater, $b_{b,w}(\lambda)$.[43,44] The $b_{b,w}(\lambda)$ values were taken as half those of the pure-seawater scattering coefficient. The absorption coefficient of the chlorophyll particles [Fig. 3(a)] at different chlorophyll a concentrations (Chl) was obtained from[45]

$$a_p(\lambda) = A_p(\lambda) Chl^{E_p(\lambda)}, \tag{8}$$

where $A_p(\lambda)$ and $E_p(\lambda)$ are empirical coefficients in the spectral range 400–700 nm. The backscattering coefficient of chlorophyll particles [Fig. 3(b)] was calculated as[46]

$$b_{b,p}(\lambda) = [0.3 Chl^{0.62} - b_w(550)]\left[0.002 + 0.02(0.5 - 0.25 \log Chl)\,\frac{550}{\lambda}\right], \tag{9}$$

where $b_w(550)$ is the scattering coefficient of pure seawater at $\lambda = 550$ nm. For our analysis we chose three values of Chl, 0.05, 0.5, and 5 mg m^{-3}, which represent low, medium, and relatively high Chl encountered in oceanic waters, respectively.

3. Results

The results are divided into three parts. First, we show how the mass-specific absorption and scattering coefficients of minerals behave as the refractive index and the size distribution change. Second, we show the variability in $b_b(\lambda)/[a(\lambda) + b_b(\lambda)]$ for two distinct cases: (1) when the mineral particles are the only particulate constituent of seawater and (2) when the minerals are accompanied by chlorophyll particles. Finally, we use the modeled spectra of $b_b(\lambda)/[a(\lambda) + b_b(\lambda)]$ as input to the standard algorithms for estimating chlorophyll from reflectance to show the degradation of the performance of these algorithms in response to variations in the properties and concentrations of suspended minerals.

A. Mass-Specific Absorption and Backscattering Coefficients of Minerals

The Mie calculations for mineral particles were performed for different combinations of n, j, and n'. To facilitate the presentation of results, we assumed that the base composition of minerals (hereafter referred to as the base mineral model) is described by $n = 1.18$ and $j = -4$. The base model involves two versions: one corresponds to weakly absorbing minerals (low-n' case), and the other corresponds to strongly absorbing minerals (high-n' case). The re-

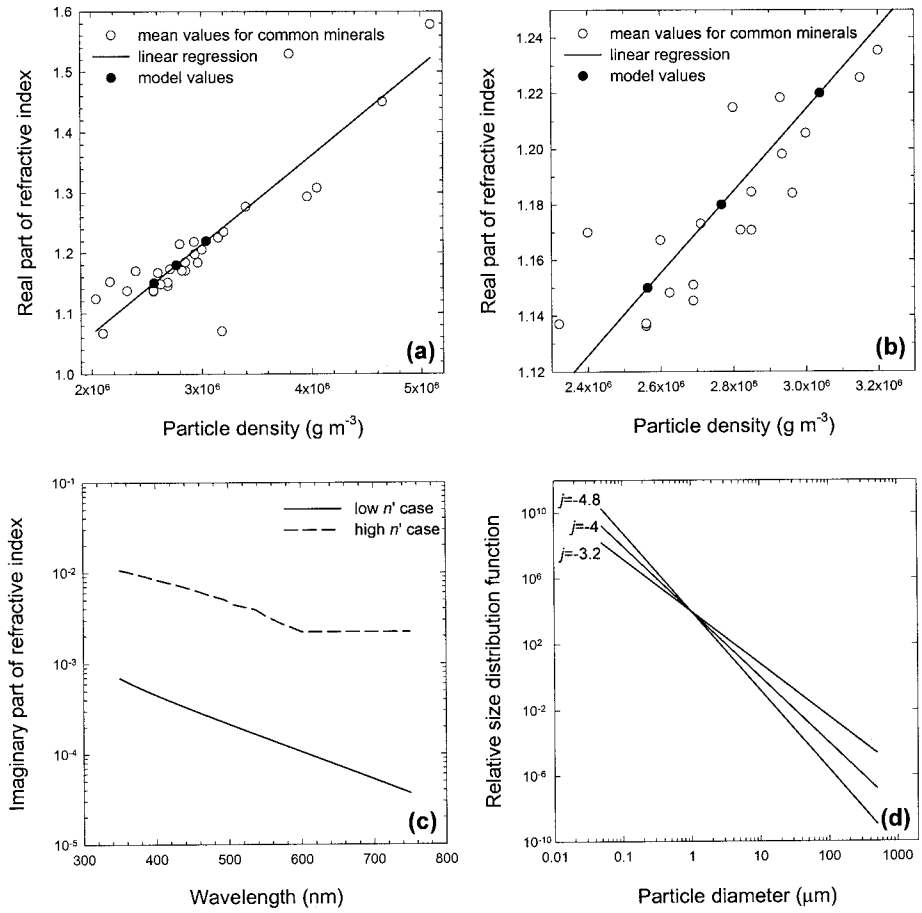

Fig. 2. Input data for the Mie scattering calculations for mineral particles. (a) and (b) Real part of the refractive index (relative to water) versus particle density for different mineral species. Open circles, data from Table 1; solid line, the best-fit linear regression; filled circles, the three values selected for our modeling. (c) Spectra of the imaginary part of the refractive index(relative to water) used in our modeling. Solid line and dashed curve represent the low- and high-n' cases, respectively. (d) Junge-type differential size distribution of particles with the three values of slope j used in our modeling.

sults for n and j that are higher and lower than the base values of $n = 1.18$ and $j = -4$ are used to illustrate the variations in the optical properties of minerals. We also show how sensitive the results are to the assumptions of a smaller refractive-index value ($n = 1.12$ for $j = -4$ and high n') and smaller $D_{\max}$ values (50 and 10 μm for $j = -4$ and high n').

The mass-specific absorption coefficient $a_m^*(\lambda)$ is obviously higher for the high-n' case than for the low-n' case [Fig. 4(a)]. The influence of n on $a_m^*(\lambda)$ is small in both cases of n'. For high n', $a_m^*(\lambda)$ decreases less than 7% when n increases from 1.18 to 1.22. When n decreases to 1.15, $a_m^*(\lambda)$ increases less than 6%. For low n', the range of changes induced by n is ±6%. For the smallest value of n considered ($n = 1.12$), the $a_m^*(\lambda)$ values are as much as 12% higher than those from the base model. The influence of j on $a_m^*(\lambda)$ is significant [Fig. 4(b)]. When $j = -3.2$, large particles are relatively more abundant compared with steeper-sloped size distributions. For high n', the package effect associated with large particles for $j = -3.2$ is capable of reducing $a_m^*(\lambda)$ by more than an order of magnitude compared with that for steeper slopes. For low n', the effect of j on $a_m^*(\lambda)$ is smaller but remains important in the blue part of the spectrum. These results support the conclusion that the package effect associated with an increased relative abundance of large particles is more pronounced when particles exhibit strong absorption.[47,48] Additional calculations for the smaller values of $D_{\max}$ (10 and 50 μm) show that a decrease in $D_{\max}$ results in an increase in $a_m^*(\lambda)$. This could be expected owing to a reduction of the package effect.

Our calculations suggest that the magnitude of $a_m^*(\lambda)$ may exhibit considerable variations over more than an order of magnitude. Near 400 nm, $a_m^*(\lambda)$ can be less than 0.01 $m^2\ g^{-1}$ for low n' and slightly greater than 0.1 $m^2\ g^{-1}$ for high n'. This variation encompasses the range of $a_m^*(\lambda)$ values determined from laboratory measurements on mineral-dominated particulate assemblages suspended in water.[1,2] Babin and Stramski[1] observed the variation in $a_m^*(400)$ between 0.05 and 0.64 $m^2\ g^{-1}$ for soil dust samples from northern Africa and Kuwait, including Saharan dust collected in southern France. Stramski *et al.*[2] measured $a_m^*(400)$ be-

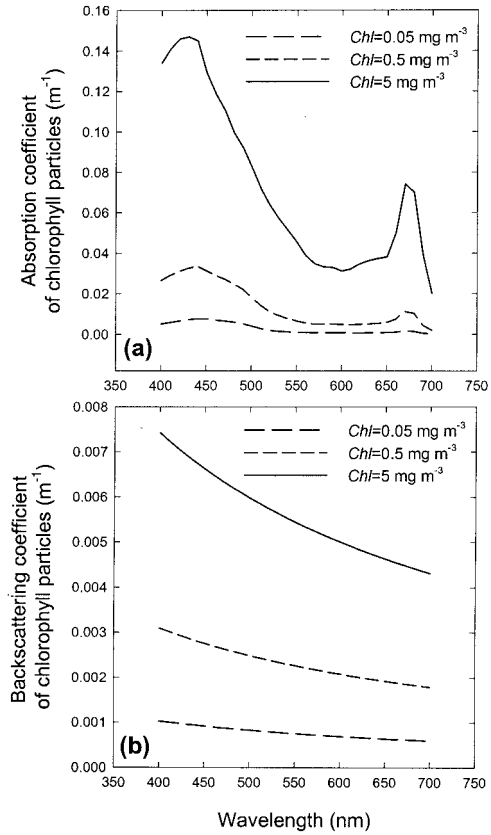

Fig. 3. (a) Absorption coefficient of chlorophyll particles according to the empirical formula from Bricaud *et al.*[45] for the three chlorophyll *a* concentrations, $Chl = 0.05$ mg m^{-3}, $Chl = 0.5$ mg m^{-3}, and $Chl = 5$ mg m^{-3}. (b) As (a), but for the backscattering coefficient according to the formula given by Morel.[46]

tween 0.05 and 0.23 m^2 g^{-1} for samples of Asian mineral dust. Within the range of our modeled a_m* are also estimates of a_m*(λ) (0.038 m^2 g^{-1} at 400 nm) obtained from measurements of particulate absorption in the Irish Sea.[49]

The effects of n' on the mass-specific backscattering coefficient, $b_{b,m}$*(λ), are less important than those for the absorption. However, $b_{b,m}$*(λ) is highly sensitive to variations in n and j [Figs. 4(c) and 4(d)]. The $b_{b,m}$*(λ) values increase with increasing n. The change of n from 1.15 to 1.22 may induce nearly a twofold increase in $b_{b,m}$*(λ). For $n = 1.12$, $b_{b,m}$*(λ) is reduced by as much as 53% compared with the base value of $n = 1.18$ (for $j = -4$ and high n'). The effect of size distribution on $b_{b,m}$*(λ) can be even greater. Compared with the base set of parameters ($n = 1.18$ and $j = -4$), $b_{b,m}$*(λ) increases approximately 2–3 times if the slope j changes from −4 to −4.8. For $j = -3.2$, $b_{b,m}$*(λ) decreases dramatically. For example, when $n = 1.18$, the $b_{b,m}$* value at 400 nm is ~0.036 m^2 g^{-1} for $j = -4.8$ and only in the range 0.0003–0.0006 m^2 g^{-1} for $j = -3.2$ at high n' and low n', respectively. If $j = -4$, the decrease in $D_{\max}$ from 500 to 10 μm results in an increase in $b_{b,m}$*(λ) by as much as 74%. These results indicate that an increase in the relative abundance of very small particles that correspond to steeper-slope j or lower $D_{\max}$ makes a stronger contribution to backscattering than to the total mass of the particles.

To our knowledge, no measurements of backscattering by mineral particles suspended in water are available for comparison with our modeled backscattering coefficients. However, we can make such a comparison for the total scattering coefficient [Figs. 4(e) and 4(f)]. For example, for most of our calculations with $D_{\max} = 500$ μm, the values of the mass-specific scattering coefficient b_m*(555) range from ~0.27 to 0.36 m^2 g^{-1}. For $j = -3.2$, however, b_m*(λ) is reduced by an order of magnitude compared with the values reported above. The b_m* values of 0.3–0.4 m^2 g^{-1} are somewhat lower than the typical estimate of 0.5 m^2 g^{-1} suggested by Babin *et al.*,[30] based on their theoretical analysis and measurements in coastal waters around Europe. Our recent laboratory measurements on suspensions of Asian mineral dust showed even higher values of b_m*(λ) (between 0.9 and 1.34 m^2 g^{-1} at 555 nm).[2] This difference can be partly due to the fact that the Asian dust samples had effectively steeper slopes of size distribution with the absence of relatively large particles compared with the particle assemblages modeled in this study. Our additional calculations with a small value of $D_{\max} = 10$ μm (for $j = -4$, $n = 1.18$, and high n') predicted an increase in b_m*(555) to a value of 0.52 m^2 g^{-1}. Because this calculated value is still lower than the experimental data for Asian mineral dust, the difference can be attributed (at least in part) to the assumptions of the model (i.e., a single slope j and a homogeneous sphere model with a single value of the refractive index for all particle sizes).

The backscattering ratio, b_m*(λ)/$b_{b,m}$*(λ), for the base model calculations ranged between 0.025 and 0.044. The range of b_m*(λ)/$b_{b,m}$*(λ) is broader (0.02–0.08) if we consider the results for $j = -3.2$ and $j = -4.8$.

B. Variability in Ocean Reflectance Induced by Mineral Particles

Figure 5 shows the $b_b(\lambda)/[a(\lambda) + b_b(\lambda)]$ ratio for the simple case when the mineral particles are the only constituent added to pure seawater. The results for the base mineral model ($n = 1.18$ and $j = -4$) with low and high n' are shown in separate panels. The spectral curves are plotted for the five concentrations of mineral particles, $C = 0.01$, 0.1, 1, 10, and 100 g m^{-3}. These values represent a broad range of SPM in the ocean, including very high concentrations that can be observed in some coastal waters.[50] For the lowest concentration of minerals, $C = 0.01$ g m^{-3}, the spectral pattern of $b_b/(a + b_b)$ behaves in almost the same way as that for pure seawater, with the maximum near 400 nm. For $C > 0.1$ g m^{-3}, the spectra are clearly distinguishable from that corresponding to pure water. In the low-n' case [Fig. 5(a)], there is an overall increase in $b_b/(a + b_b)$ with increasing C and a tendency of the spectral maximum to shift toward longer wavelengths for the two highest values of C considered (10 g and 100 g m^{-3}). In the high-n'

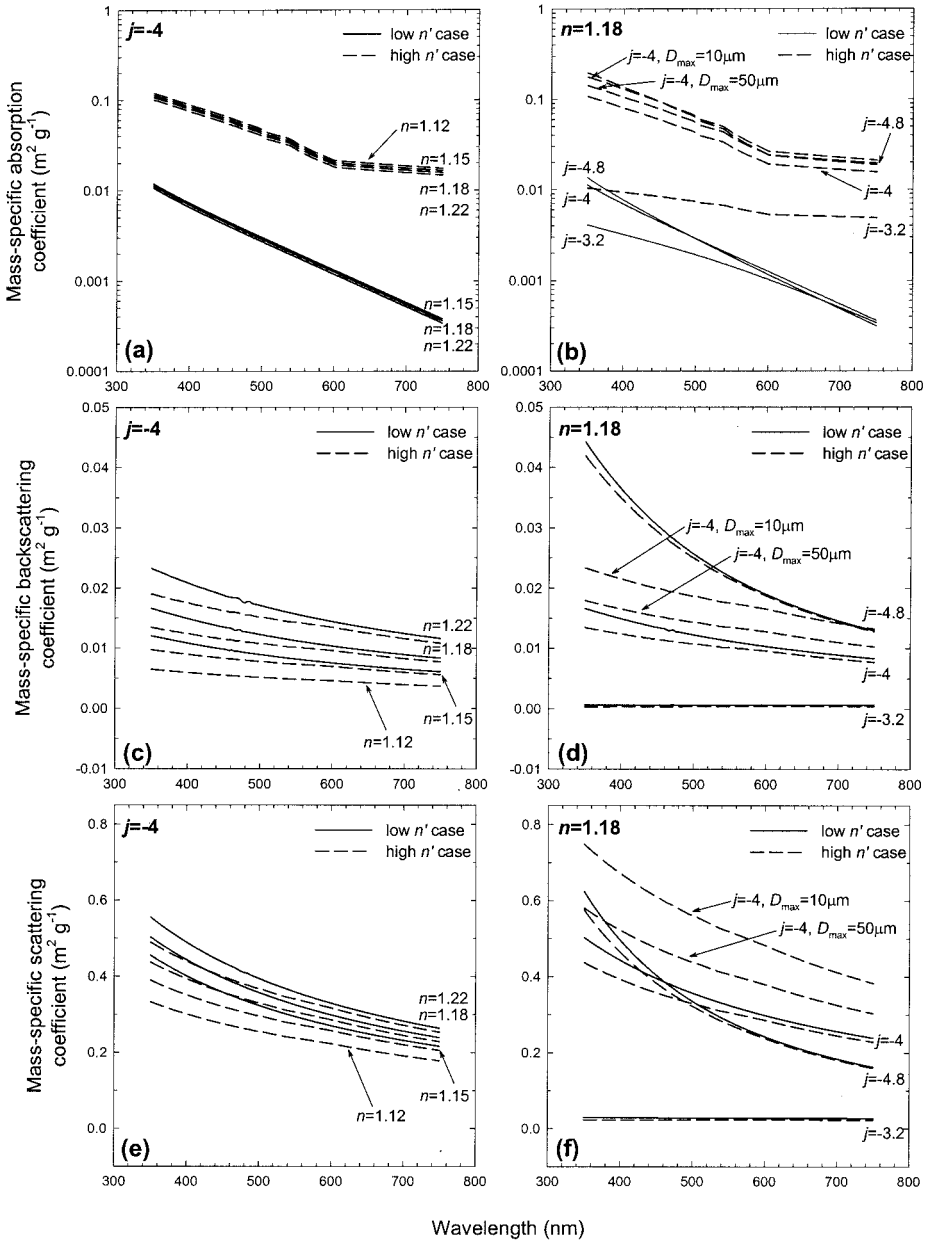

Fig. 4. (a) Effects of the real part of the refractive index, n, on the mass-specific absorption coefficient of mineral particles for a given slope of particle size distribution, $j = -4$. These effects are shown for the low-n' case (solid curves) and the high-n' case (dashed curves). (b) Effects of the slope of size distribution, j, on the mass-specific absorption coefficient of mineral particles for a given value of the real part of the refractive index, $n = 1.18$. These effects are shown for the low- and high-n' cases (solid and dashed curves, respectively). (c) and (d) As (a) and (b), but for the mass-specific backscattering coefficient of the mineral particles. (e) and (f) As (a) and (b), but for the mass-specific scattering coefficient of the mineral particles. The curves for $D_{max} = 50$ μm, $D_{max} = 10$ μm, and $n = 1.12$ are included to show the sensitivity of results to the relatively small values of D_{max} and n (see text for details).

case [Fig. 5(b)], the spectral shape of $b_b/(a + b_b)$ is flatter with smaller values overall. The values of $b_b/(a + b_b)$ decrease with increasing C within the short-wavelength region (<480 nm), and an opposite trend is seen for longer wavelengths. The shifting tendency of the spectral maximum is seen for $C \geq 1$ g m^{-3}. A similar shift of the spectral peak with increasing particle concentration was also observed in the field reflectance data.[23]

Figure 6 shows the $b_b/(a + b_b)$ ratio for n and j values that differ from the base model. The effect of variation in n is illustrated for $n = 1.15$ and $n = 1.22$ for the fixed size distribution with $j = -4$ [Figs. 6(a) and 6(b)]. This effect is reflected primarily in the more- or less-pronounced changes in the magnitude of $b_b/(a + b_b)$, with a relatively small effect on its spectral shape. In contrast, if we consider different values of j at the same refractive index $n = 1.18$, the changes in $b_b/(a + b_b)$ are more pronounced [Figs. 6(c) and 6(d)]. For $j = -3.2$ and low n', the $b_b/(a +$

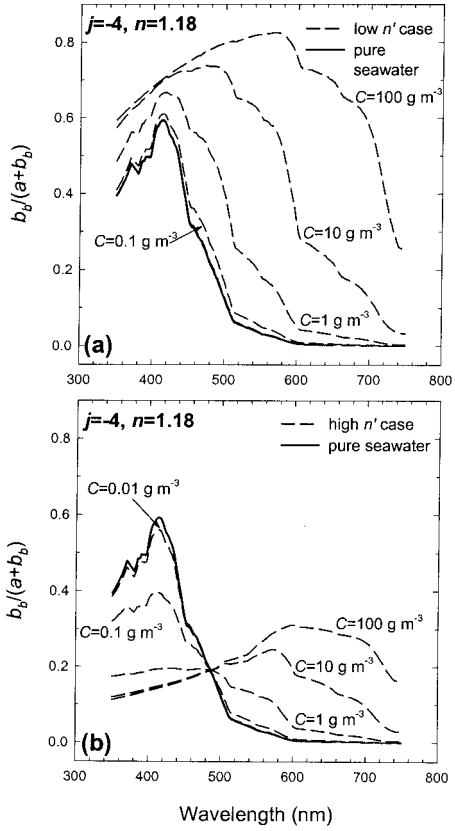

Fig. 5. Spectral curves of the $b_b/(a + b_b)$ ratio calculated for seawater with different concentrations of mineral particles that are characterized by the base values of the slope of size distribution, $j = -4$, and the real part of the refractive index, $n = 1.18$ (dashed curves). The mineral concentration is indicated by the C values: (a) represents the low-n' case and (b) represents the high-n' case. The spectral curves of the $b_b/(a + b_b)$ ratio for pure seawater are also presented in both (a) and (b) as solid curves.

b_b) values are significantly lower in comparison with the case in which $j = -4$, especially at medium-to-high particle concentrations. For example, this reduction is 40% at $C = 1$ g m^{-3} and $\lambda = 440$ nm. This is caused primarily by the small values of $b_{b,m}{}^*(\lambda)$ at $j = -3.2$ [see Fig. 2(d)]. In the high-n' case the pattern is more complex due to the interplay of the effects associated with both $a_m{}^*(\lambda)$ and $b_{b,m}{}^*(\lambda)$. At 440 nm, the gentle slope $j = -3.2$ produces an increase in $b_{b,m}{}^*$ at low-to-medium values of C (by 36% at 1 g m^{-3}) and a decrease at higher C (by 48% at 10 g m^{-3}) compared with the base value of j. In addition, for $j = -3.2$ and $n = 1.18$, the highest values of $b_b/(a + b_b)$ occur in the blue spectral region at the lowest concentration of minerals, $C = 0.01$ g m^{-3}, which is similar to the pure-seawater case. For the steep size distribution with $j = -4.8$ [Fig. 6(d)], the spectral shape of $b_b/(a + b_b)$ is similar to that for $j = -4$ [Figs. 5(a) and 5(b)]. However, if the same C and n' are compared, the magnitude of $b_b/(a + b_b)$ is generally higher at $j = -4.8$ than at $j = -4$; for example, at 440 nm, by 21% to 28% for low-n' and high-n' cases, respectively.

Figure 7 shows the $b_b/(a + b_b)$ ratio for the cases when both chlorophyll particles and mineral particles are present in seawater. The results are shown for the base mineral model ($n = 1.18$ and $j = -4$) with varying concentrations of mineral particles, C, and the three different concentrations of chlorophyll a, $Chl = 0.05$, 0.5, and 5 mg m^{-3}. At a low chlorophyll concentration ($Chl = 0.05$ mg m^{-3}) and with no minerals in water ($C = 0$), the spectral shape of $b_b/(a + b_b)$ is flatter when compared with the case of pure seawater [solid curves in Figs. 7(a) and 7(b); see also Fig. 5 for the pure-seawater case]. The observed reduction in reflectance is a well-known effect of absorption by chlorophyll in the blue spectral region. The presence of small amounts of minerals at a concentration of 0.01 g m^{-3} has virtually no effect on the $b_b/(a + b_b)$ curves, which remain indistinguishable from those corresponding to the absence of minerals in water. The increase of mineral concentration above 0.01 g m^{-3} starts to affect the $b_b/(a + b_b)$ spectra so that the effects are observed first at low Chl and then progressively at higher Chl. The mineral concentration $C = 0.1$ g m^{-3} already has a significant effect on $b_b/(a + b_b)$. As an example, for $\lambda = 440$ nm and low n', $b_b/(a + b_b)$ is 26% higher at low Chl (0.05 mg m^{-3}) and 13% higher at high Chl (5 mg m^{-3}) compared with water in which minerals are absent. Mineral concentrations of the order of 1 g m^{-3} and higher have dramatic effects on both the magnitude [for example, >200% increase in $b_b/(a + b_b)$ for the low-n' case at 440 nm] and the shape of the reflectance spectra over the entire range of Chl considered.

The $b_b/(a + b_b)$ ratio shown in Fig. 7 changes with increasing C in a manner generally similar to the simpler case with no chlorophyll in water. If minerals are weakly absorbing [Figs. 7(a), 7(c), and 7(e)], there is an overall increase of $b_b/(a + b_b)$ and a distinct change of its spectral shape with the increase in C. For $C \leq 1$ g m^{-3}, $b_b/(a + b_b)$ shows the highest values within the short-wavelength portion of the spectrum. At higher concentrations of C, a remarkable maximum develops at wavelengths between 500 and 600 nm. If minerals are highly absorbing [Figs. 7(b), 7(d), and 7(f)], the $b_b/(a + b_b)$ ratio shows generally smaller values than in the low-n' case. In addition, at low and medium Chl, the hinge point appears in the blue spectral range, which divides the spectrum into two parts. For wavelengths shorter than 420–450 nm, the reflectance decreases with increasing mineral concentration; the opposite trend is observed at wavelengths longer than the hinge point. However, the hinge point does not show up in the visible spectrum when Chl is sufficiently high [Fig. 7(f)].

The comparison of $b_b/(a + b_b)$ for different Chl values when only chlorophyll particles are present in water [e.g., solid curves in Figs. 7(a), 7(c), and 7(e)] reveals a decrease in the blue-to-green reflectance ratio with increasing Chl, which is used in most of the present-day algorithms for chlorophyll estimation from ocean color measurements.[51] However, Fig. 7

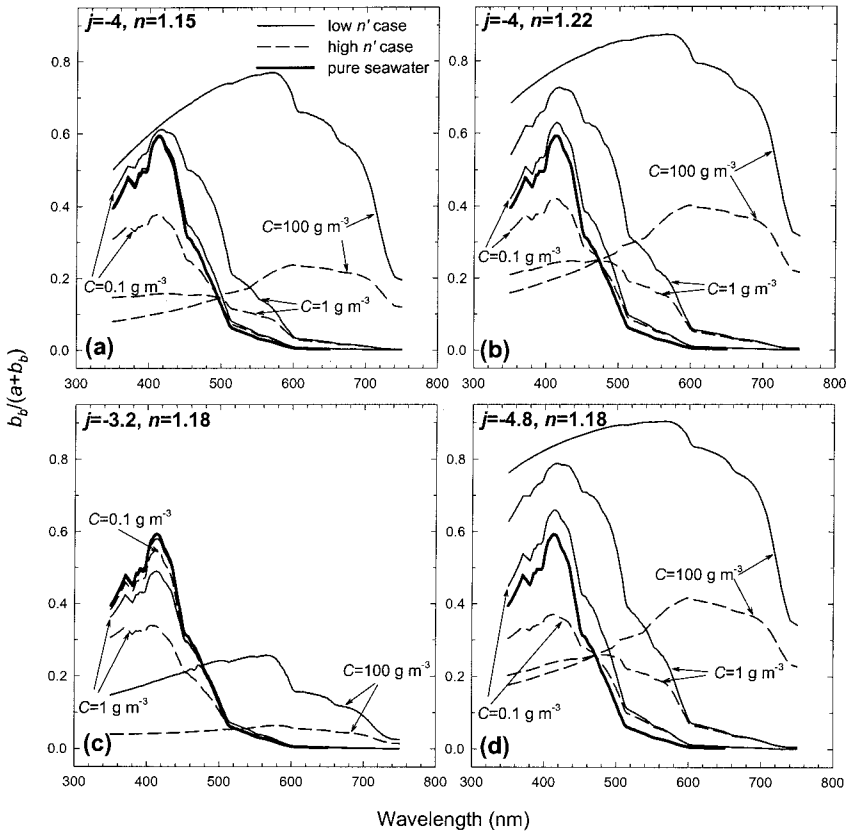

Fig. 6. Spectral curves of the $b_b/(a + b_b)$ ratio calculated for seawater with different concentrations of mineral particles, C, for four combinations of the slope of size distribution, j, and the real part of the refractive index, n (the relevant values are indicated in each panel). The thin solid curves represent the low-n' case and the dashed curves the high-n' case. Pure seawater is shown as the thick solid curve.

also shows that the slope of the reflectance spectrum in the blue–green spectral region can change significantly with varying concentration and properties of mineral particles. This indicates that the presence of minerals introduces errors in chlorophyll estimates from the blue-to-green reflectance ratio.

C. Effects of Mineral Particles on the Chlorophyll Estimation

For testing the influence of mineral particles on the chlorophyll estimation from ocean color, we examine the standard NASA global algorithms that are used in conjunction with satellite missions of SeaWiFS and MODIS sensors.[52,53] Specifically, we examine the chlorophyll algorithms known as OC2, OC4, and chlor_MODIS, which are described by the functional form[54,55]

$$Chl = 10^{(a_0+a_1R_r+a_2R_r^2+a_3R_r^3)} + a_4, \qquad (10)$$

where R_r is the spectral band ratio either of the remote-sensing reflectance or the normalized water-leaving radiance utilized by a particular algorithm and a_0, a_1, a_2, a_3, a_4 are the empirical coefficients (see Table 2 for details).

From the above-described spectra of $b_b/(a + b_b)$ for different combinations of mineral properties (n, n', and j), mineral particle concentration, C, and chlorophyll concentration, Chl, we calculated the band ratios needed as input to the chlorophyll algorithms. The algorithm calculations with this input allow us to compare the values of Chl estimated for the situations when both the mineral and chlorophyll particles are present in water with Chl estimates when only chlorophyll particles are present. The analysis of the ratio of these two types of Chl estimates shows how the chlorophyll algorithms are affected by different properties and by concentrations of mineral assemblages at different chlorophyll concentrations.

The ratio of Chl estimates from the OC2 algorithm indicates that the potential errors in Chl depend not only on the concentration but also on the size distribution and refractive index of mineral particles (Fig. 8). The errors are largest at low Chl [Fig. 8(a)]. The increase in C results in an increased overestimation of OC2-derived Chl, which can reach tens to hundreds of percent or more in extreme situations. At a given C, the magnitude of this overestimation depends on the properties of mineral assemblages; most notably, the overestimation is significantly larger for steeper size distributions. When Chl is low, the weakly absorbing minerals (the low-n' case) at an example concentration $C = 1$ g m^{-3} cause a 3- to 4-fold overestimation of Chl for the various combinations of n and j, with the exception of $j = -3.2$, for which the overestimation is 1.5-fold. The effect of

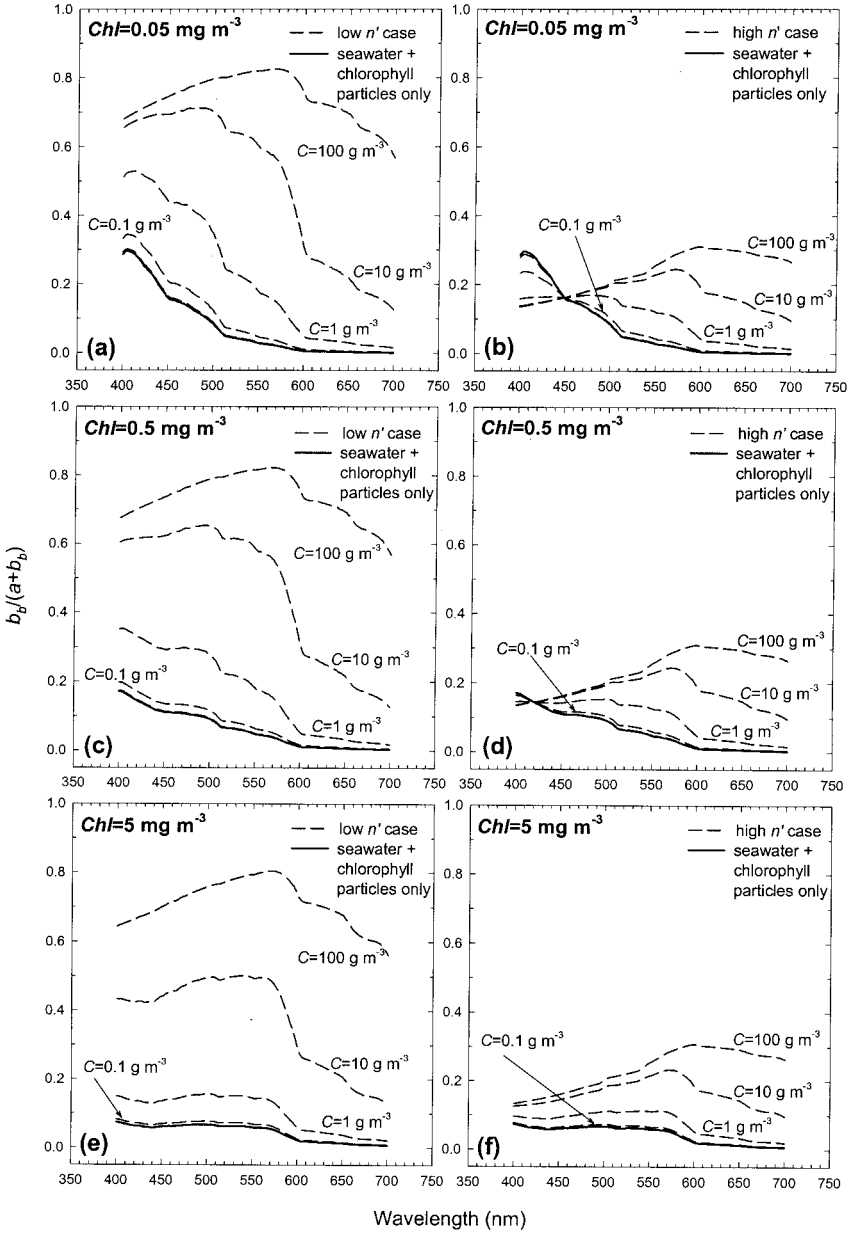

Fig. 7. Spectral curves of the $b_b/(a + b_b)$ ratio for the various cases when mineral particles at different concentrations C are accompanied by the presence of chlorophyll particles at low [(a) and (b)], medium [(c) and (d)], and high [(e) and (f)] chlorophyll a concentrations, as indicated by the values of Chl. The mineral particles are characterized by the base values of the slope of the size distribution, $j = -4$, and the real part of the refractive index, $n = 1.18$. The left-hand panels are for the low-n' case, and the right-hand panels are for the high-n' case. The solid curves represent seawater with chlorophyll particles only (no minerals in water).

Table 2. Band Ratios and Coefficients of Standard Chlorophyll Algorithms[a]

Algorithm	Band Ratio	Empirical Coefficients				
		a_0	a_1	a_2	a_3	a_4
OC2	$R_r = \log[R_{rs}(490)/R_{rs}(555)]$	0.341	−3.001	2.811	−2.041	−0.04
OC4	$R_r = \log\{\max[R_{rs}(443), R_{rs}(490), R_{rs}(510)]/R_{rs}(555)\}$	0.4708	−3.8469	4.5338	−2.2234	−0.0414
chlor_MODIS	$R_r = \log\{[L_{wn}(442.1) + L_{wn}(486.9)]/L_{wn}(546.8)\}$					
	for $R_r > 0.9866$	0.8904	−3.911	4.7122	−2.8237	0
	for $R_r \le 0.9866$	0.8791	−6.0171	12.0707	−8.1067	0

[a] R_{rs} is the remote-sensing reflectance (in sr^{-1}), and L_{wn} is the normalized water-leaving radiance (in $W\ m^{-2}\ nm^{-1}\ sr^{-1}$).

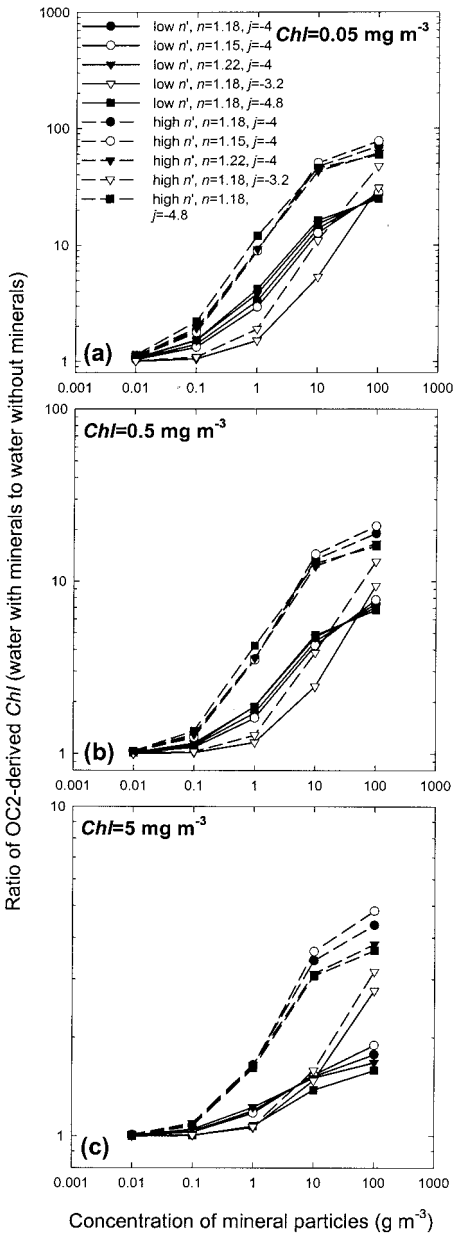

Fig. 8. Ratio of *Chl* estimated from the OC2 algorithm when minerals are present in water to *Chl* estimated with no minerals in water as a function of mineral particle concentration. (a) The low concentration of chlorophyll *a*, $Chl = 0.05$ mg m^{-3}; (b) the medium pigment concentration, $Chl = 0.5$ mg m^{-3}; and (c) the relatively high pigment concentration, $Chl = 5$ mg m^{-3}. The size distribution and refractive-index parameters that define the mineral particle assemblages are shown in (a).

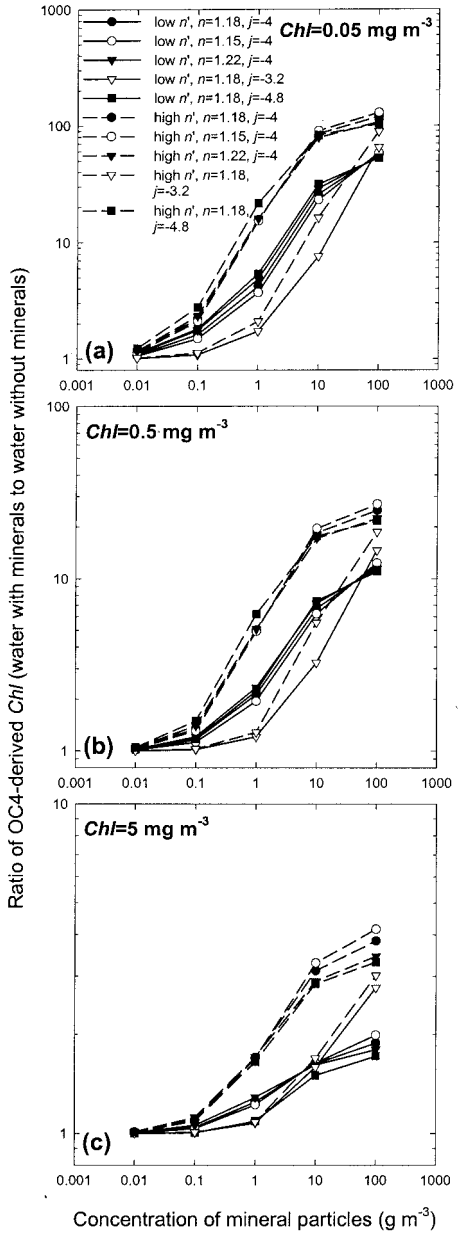

Fig. 9. Same as Fig. 8, but for the OC4 algorithm.

strongly absorbing minerals (the high-n' case) is even greater because *Chl* at the same $C = 1$ g m^{-3} may be overestimated by a factor that is higher than 10, and only the gentle slope $j = -3.2$ gives a considerably smaller overestimation (by a factor of 1.9). For the examined ranges of n, n', and j, the changes in the real part of the refractive index appear to have a smaller effect on the *Chl* estimation compared with those of the size distribution and absorption of mineral particles.

For higher chlorophyll concentrations, the *Chl* overestimation is smaller, which means that larger amounts of mineral particles are generally needed to give the same level of error with increasing *Chl* [Figs. 8(b) and 8(c)]. As an example, for $Chl = 0.5$ mg m^{-3}, the presence of minerals at the concentration of 1 g m^{-3} may result in an OC2-derived *Chl* that overestimates the actual *Chl* by a factor as high as 4.2. For *Chl* of 5 mg m^{-3}, the corresponding overestimation is by a factor of $\sim$1.7. The general features associated with the effects of mineral properties observed for low *Chl* also persist for higher *Chl*. Because the slope of the size distribution is steeper or the absorption of

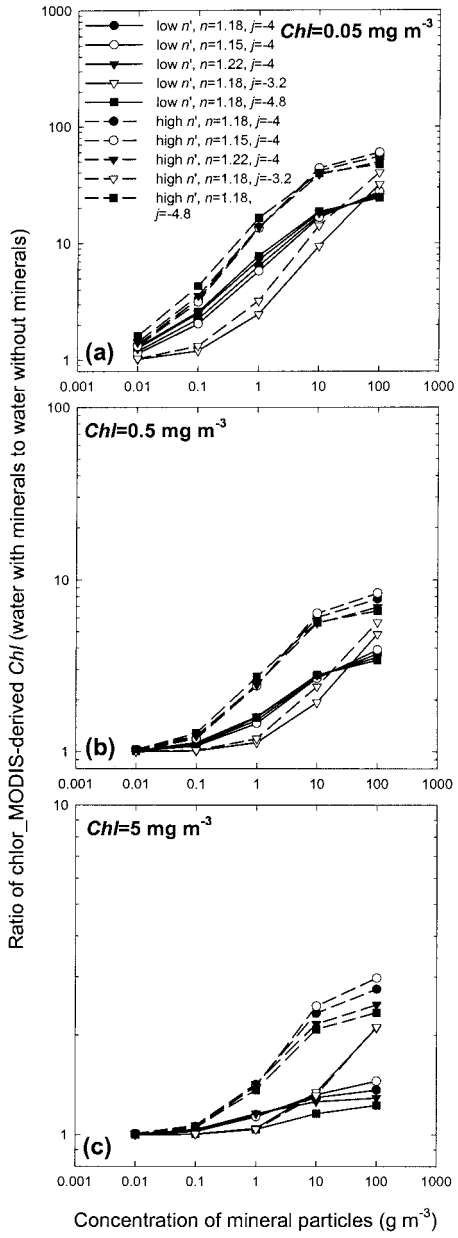

Fig. 10. Same as Fig. 8, but for the chlor_MODIS algorithm.

mineral particles is stronger, the errors in *Chl* estimates increase. This is because the mass-specific backscattering of minerals is higher for steeper slopes j and the mass-specific absorption of minerals increases with n' (see Fig. 4). At any given C, this leads to the enhanced contribution of minerals to the blue-to-green reflectance ratio and to the degradation of the performance of chlorophyll algorithms. The effect of the real part of the refractive index of minerals on these algorithms cannot be totally ignored, however. For example, at $Chl = 0.5$ mg m^{-3}, $C = 1$ g m^{-3}, and $j = -4$, the change of n from 1.15 to 1.22 produces an increase in the ratio of chlorophyll estimates of ~16% and 2% at low and high n', respectively.

Figures 9 and 10 show results similar to those in Fig. 8, but for the OC4 and chlor_MODIS algorithms, respectively. The results for OC4 are very similar to those for the OC2 algorithm. Compared with other algorithms, chlor_MODIS shows somewhat higher sensitivity to the presence of minerals at low chlorophyll concentrations [Fig. 10(a)] and generally a little lower sensitivity for the medium and high chlorophyll concentrations [Figs. 10(b) and 10(c)].

Some cases presented in Figs. 8–10 are rather extreme. Obviously, the very high concentrations of minerals of the order of 100 g m^{-3} modify the reflectance spectra to such a great extent that standard remote-sensing algorithms for chlorophyll are useless. However, even the low and medium concentrations of mineral particles of the order of 0.1 to 1 g m^{-3} should be considered as a potential source of significant error in the chlorophyll estimation. For low and medium *Chl* encountered in most open ocean waters (less than ~0.5 mg m^{-3}), the mineral concentration of the order of 0.1 g m^{-3} has the potential to cause an overestimation of *Chl* of as high as 100%. For higher chlorophyll concentrations such effects are possible when minerals are present in seawater at concentrations of the order of 1 g m^{-3} or higher.

4. Conclusions

Mineral particles suspended in seawater in concentrations of O(0.1) g m^{-3} or higher have significant influence on ocean reflectance. The particle concentrations of 1 g m^{-3} or higher can completely change the magnitude and spectral shape of the reflectance in comparison with clear ocean water. To understand the influences of minerals on ocean reflectance, one must take into account not only the mass concentration of particles but also the particle size distribution and the complex refractive index that are dependent on the composition of particles. These particle properties affect the mass-specific absorption and backscattering coefficients, which in turn produce variations in the ocean reflectance at the same concentration of mineral particles. The imaginary part of the refractive index and size distribution are especially important because different combinations of n' and j produce quite different spectral patterns of ocean reflectance.

The chlorophyll estimation from standard SeaWiFS and MODIS algorithms may be significantly affected even by relatively low concentrations of mineral particles of the order of 0.1 g m^{-3}. The increase in the concentration of suspended minerals causes an increase in the overestimation of the algorithm-derived chlorophyll concentration. When real chlorophyll concentrations are low (of the order of 0.05 mg m^{-3}), the mineral concentration of ~1 g m^{-3} may introduce a chlorophyll overestimation of as much as 20 times when the OC2, OC4, and chlor_MODIS algorithms are used. This suggests that, even in open ocean waters, the relatively small amounts of suspended minerals associated, for example, with dust deposition from the atmosphere[2,26] can

be a source of significant error in the remote sensing of phytoplankton pigments.

This work was supported by the Environmental Optics Program of the U.S. Office of Naval Research (grant N00014-98-1-0003 to D. Stramski) and the NSF–NATO Postdoctoral Fellowship in Science and Engineering (grant DGE-0108025 to S. B. Woźniak and D. Stramski). Partial support was also provided by the Polish National Committee for Scientific Research (grant PBZ-KBN 056/P04/2001). We thank P. Curran and two anonymous reviewers for their comments on the manuscript.

References

1. M. Babin and D. Stramski, "Variations in the mass-specific absorption coefficient of mineral particles suspended in water," Limnol. Oceanogr. **49,** 756–767 (2004).
2. D. Stramski, S. B. Woźniak, and P. J. Flatau, "Optical properties of Asian mineral dust suspended in seawater," Limnol. Oceanogr. **49,** 749–755 (2004).
3. R. J. Gibbs, "Transport phases of transition metals in the Amazon and Yukon Rivers," Geol. Soc. Am. Bull. **88,** 829–843 (1977).
4. B. G. Li, D. Eisma, Q. Ch. Xie, J. Kalf, Y. Li, and X. Xia, "Concentration, clay mineral composition and Coulter counter size distribution of suspended sediment in the turbidity maximum of the Jiaojiang river estuary, Zhejiang, China," J. Sea Res. **42,** 105–116 (1999).
5. J. M. Prospero, "Mineral–aerosol transport to the North Atlantic and North Pacific: the impact of African and Asian sources," in *The Long Range Atmospheric Transport of Natural and Contaminant Substances*, A. H. Knap, ed. (Kluwer Academic, Dordrecht, The Netherlands, 1990), pp. 59–86.
6. A. Morel and L. Prieur, "Analysis of variations in ocean color," Limnol. Oceanogr. **40,** 709–722 (1977).
7. H. R. Gordon and A. Morel, *Remote Assessment of Ocean Color for Interpretation of Satellite Visible Imagery—a Review. Lecture Notes on Coastal and Estuarine Studies* (Springer-Verlag, New York, 1983).
8. E. M. M. Novo, J. D. Hanson, and P. J. Curran, "The effect of sediment type on the relationship between reflectance and suspended sediment concentration," Int. J. Remote Sens. **10,** 1283–1289 (1989).
9. Z. Chen, P. J. Curran, and J. D. Hansom, "Derivative reflectance spectroscopy to estimate suspended sediment concentration," Remote Sens. Environ. **40,** 67–77 (1992).
10. L. Han, "Spectral reflectance with varying suspended sediment concentrations in clear and algae-laden waters," Photogramm. Eng. Remote Sens. **63,** 701–705 (1997).
11. G. F. Moore, J. Aiken, and S. J. Lavender, "The atmospheric correction of water colour and the quantitative retrieval of suspended particulate matter in case II waters: application to MERIS," Int. J. Remote Sens. **20,** 1713–1733 (1999).
12. K. Y. H. Gin, S. T. Koh, and I. I. Lin, "Study of the effects of suspended marine clay on the reflectance spectra of phytoplankton," Int. J. Remote Sens. **23,** 2163–2178 (2002).
13. R. P. Stumpf and J. R. Pennock, "Calibration of a general optical equation for remote sensing of suspended sediments in a moderately turbid estuary," J. Geophys. Res. **94,** 14363–14371 (1989).
14. P. J. Curran, J. D. Hansom, S. E. Plummer, and M. I. Pedley, "Multispectral remote sensing of nearshore suspended sediments: a pilot study," Int. J. Remote Sens. **8,** 103–112 (1987).
15. Y.-H. Ahn, J. Moon, and S. Gallegos, "Development of suspended particulate matter algorithms for ocean color remote sensing," Korean J. Remote Sens. **17,** 285–295 (2001).
16. D. Doxaran, J.-M. Froidefond, and P. Castaing, "A reflectance band ratio used to estimate suspended matter concentrations in sediment-dominated coastal waters," Int. J. Remote Sens. **23,** 5079–5085 (2002).
17. J. Fisher and R. Doerffer, "An inverse technique for remote detection of suspended matter, phytoplankton and yellow substance from CZCS measurements," Adv. Space Res. **7,** 21–26 (1987).
18. S. Sathyendranath, L. Prieur, and A. Morel, "A three-component model of ocean colour and its application to remote sensing of phytoplankton pigments in coastal waters," Int. J. Remote Sens. **10,** 1373–1394 (1989).
19. S. Tassan, "Local algorithms using SeaWiFS data for the retrieval of phytoplankton, pigments, suspended sediment, and yellow substance in coastal waters," Appl. Opt. **33,** 2369–2378 (1994).
20. F. Lahet, S. Ouillon, and P. Forget, "A three-component model of ocean color and its application in the Ebro river mouth area," Remote Sens. Environ. **72,** 181–190 (2000).
21. R. W. Gould, Jr. and R. A. Arnone, "Remote sensing estimates of inherent optical properties in a coastal environment," Remote Sens. Environ. **61,** 290–301 (1997).
22. P. Forget, S. Ouillon, F. Lahet, and P. Broche, "Inversion of reflectance spectra of nonchlorophyllous turbid coastal waters," Remote Sens. Environ. **68,** 264–272 (1999).
23. D. Doxaran, J.-M. Froidefond, S. Lavender, and P. Castaing, "Spectral signature of highly turbid waters. Application with SPOT data to quantify suspended particulate matter concentrations," Remote Sens. Environ. **81,** 149–161 (2002).
24. R. P. Stumpf and J. R. Pennock, "Remote estimation of the diffuse attenuation coefficient in a moderately turbid estuary," Remote Sens. Environ. **38,** 183–191 (1991).
25. M. Sydor and R. A. Arnone, "Effect of suspended particulate and dissolved organic matter on remote sensing of coastal and riverine waters," Appl. Opt. **36,** 6905–6912 (1997).
26. H. Claustre, A. Morel, S. B. Hooker, M. Babin, D. Antoine, K. Oubelkheir, A. Bricaud, K. Leblanc, B. Queguiner, and S. Maritorena, "Is desert dust making oligotrophic waters greener?" Geophys. Res. Lett. **29,** 10.1029/2001GL014056 (2002).
27. C. F. Bohren and D. R. Huffman, *Absorption and Scattering of Light by Small Particles* (Wiley, New York, 1983).
28. A. Morel and A. Bricaud, "Inherent optical properties of algal cells including picoplankton: theoretical and experimental results," in *Photosynthetic Picoplankton*, T. Platt and W. K. W. Li, eds., Can. Bull. Fish. Aquat. Sci. **214,** 521–559 (1986).
29. A. Bricaud and A. Morel, "Light attenuation and scattering by phytoplanktonic cells: a theoretical modeling," Appl. Opt. **25,** 571–580 (1986).
30. M. Babin, A. Morel, V. Fournier-Sicre, F. Fell, and D. Stramski, "Light scattering properties of marine particles in coastal and open ocean waters as related to the particle mass concentration," Limnol. Oceanogr. **48,** 843–859 (2003).
31. H. R. Gordon, O. B. Brown, and M. M. Jacobs, "Computed relationships between inherent and apparent optical properties of a flat, homogeneous ocean," Appl. Opt. **14,** 417–427 (1975).
32. A. Morel and B. Gentili, "Diffuse reflectance in oceanic waters. II. Bidirectional aspects," Appl. Opt. **32,** 6864–6879 (1993).
33. R. A. Reynolds, D. Stramski, and B. G. Mitchell, "A chlorophyll-dependent semianalytical reflectance model derived from field measurements of absorption and backscattering coefficients within the Southern Ocean," J. Geophys. Res. **106,** 7125–7138 (2001).
34. P. F. Kerr, *Optical Mineralogy* (McGraw-Hill, New York, 1977).
35. L. G. Berry and B. Mason, *Mineralogy: Concepts, Descriptions, Determinations* (Freeman, San Francisco, 1959).

36. I. N. Sokolik and O. B. Toon, "Incorporation of mineralogical composition into models of the radiative properties of mineral aerosol from UV to IR wavelengths," J. Geophys. Res. **104,** 9423–9444 (1999).
37. D. Stramski, A. Bricaud, and A. Morel, "Modeling the inherent optical properties of the ocean based on the detailed composition of the planktonic community," Appl. Opt. **40,** 2929–2945 (2001).
38. E. M. Patterson, D. A. Gillette, and B. H. Stockton, "Complex index of refraction between 300 and 700 nm for Saharan dust," J. Geophys. Res. **82,** 3153–3160 (1997).
39. H. Bader, "The hyperbolic distribution of particle size," J. Geophys. Res. **75,** 2822–2830 (1970).
40. D. Stramski and D. A. Kiefer, "Light scattering by microorganisms in the open ocean," Prog. Oceanogr. **28,** 343–383 (1991).
41. R. M. Pope and E. S. Fry, "Absorption spectrum (380–700 nm) of pure water. II. Integrating cavity measurements," Appl. Opt. **36,** 8710–8723 (1997).
42. F. M. Sogandares and E. S. Fry, "Absorption spectrum (340–640 nm) of pure water. I. Photothermal measurements," Appl. Opt. **36,** 8699–8709 (1997).
43. R. C. Smith and K. S. Baker, "Optical properties of the clearest natural waters (200–800 nm)," Appl. Opt. **20,** 177–184 (1981).
44. A. Morel, "Optical properties of pure water and pure sea water," in *Optical Aspects of Oceanography*, N. G. Jerlov and E. Steemann Nielsen, eds. (Academic, London, 1974), pp. 1–24.
45. A. Bricaud, A. Morel, M. Babin, K. Allali, and H. Claustre, "Variations of light absorption by suspended particles with chlorophyll a concentration in oceanic (case 1) waters: Analysis and implications for bio-optical models," J. Geophys. Res. **103,** 31033–31044 (1998).
46. A. Morel, "Optical modeling of the upper ocean in relation to its biogenous matter content (case-I waters)," J. Geophys. Res. **93,** 10749–10768 (1988).
47. L. N. M. Duysens, "The flattening of the absorption spectrum of suspensions as compared to that of solutions," Biochim. Biophys. Acta **19,** 1–12 (1956).
48. A. Morel and A. Bricaud, "Theoretical results concerning light absorption in a discrete medium, and application to specific absorption of phytoplankton," Deep-Sea Res. **28,** 1375–1393 (1981).
49. D. G. Bowers, G. E. L. Harker, and B. Stephan, "Absorption spectra of inorganic particles in the Irish Sea and their relevance to remote sensing of chlorophyll," Int. J. Remote Sens. **17,** 2449–2460 (1996).
50. D. Eisma, *Suspended Matter in the Aquatic Environment* (Springer-Verlag, Berlin, 1993).
51. J. E. O'Reilly, S. Maritorena, B. G. Mitchell, D. A. Siegel, K. E. Carder, S. A. Garver, M. Kahru, and C. McClain, "Ocean color chlorophyll algorithms for SeaWiFS," J. Geophys. Res. **103,** 24937–24953 (1998).
52. S. B. Hooker and C. R. McClain, "The calibration and validation of SeaWiFS data," Prog. Oceanogr. **45,** 427–465 (2000).
53. W. E. Esaias, M. R. Abbott, I. Barton, O. B. Brown, J. W. Campbell, K. L. Carder, D. K. Clark, R. H. Evans, F. E. Hoge, H. R. Gordon, W. M. Balch, R. Letelier, and P. J. Minnett, "An overview of MODIS capabilities for ocean science observations," IEEE Trans. Geosci. Remote Sens. **36,** 1250–1265 (1998).
54. J. E. O'Reilly, S. Maritorena, D. A. Siegel, M. C. O'Brien, D. Toole, B. G. Mitchell, M. Kahru, F. P. Chavez, P. Strutton, G. F. Cota, S. B. Hooker, C. R. McClain, K. L. Carder, F. Müller-Karger, L. Harding, A. Magnuson, D. Phinney, G. F. Moore, J. Aiken, K. R. Arrigo, R. Letelier, and M. Culver, "Ocean color chlorophyll algorithms for SeaWiFS, OC2, and OC4: Version 4," in *SeaWiFS Postlaunch Calibration and Validation Analyses, Part 3*, S. B. Hooker and E. R. Firestone, eds. NASA Tech. Memo. 2000–206892 (NASA, Greenbelt, Md., 2000), Vol. 11, pp. 9–27.
55. D. K. Clark, Oceanic Research and Applications Division, National Oceanic and Atmospheric Administration, Camp Springs, Md. 20746 (personal communication, 2002).